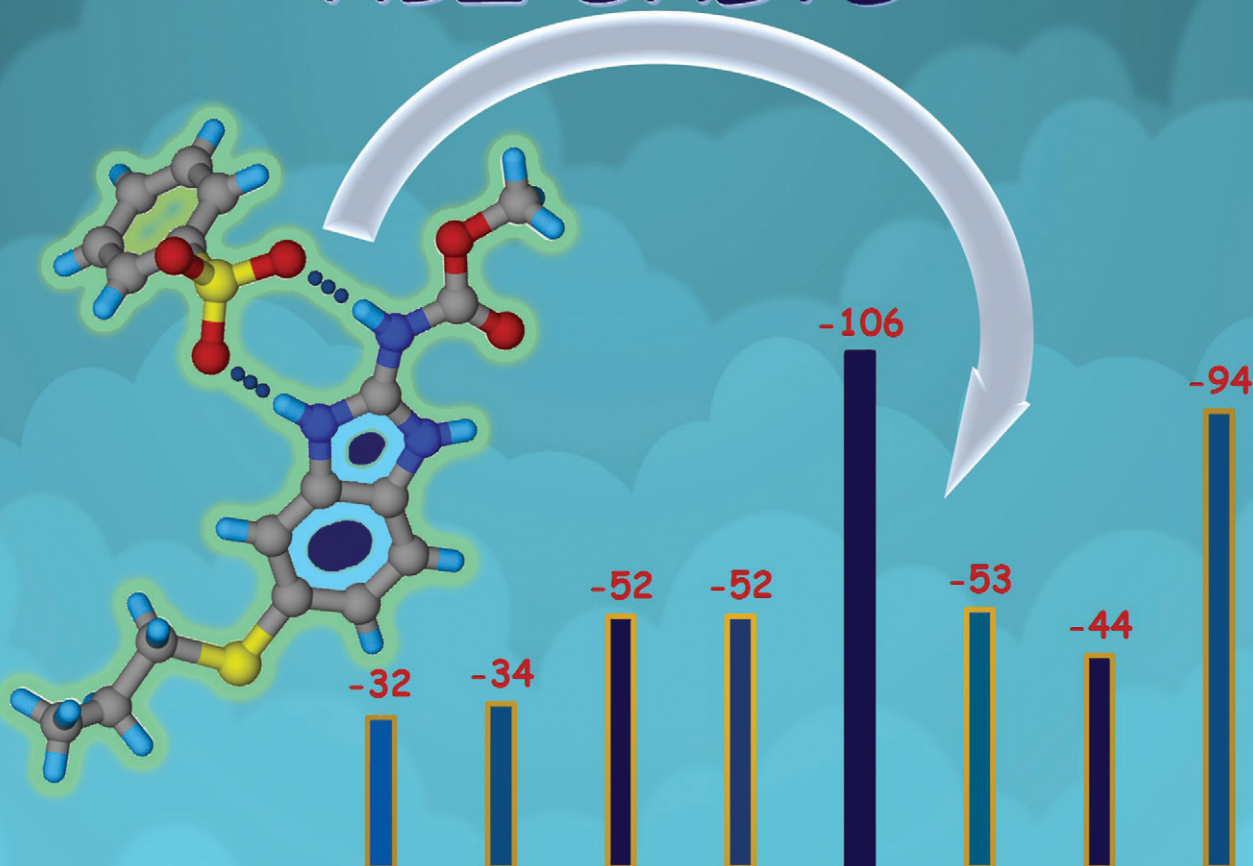# ABZ SALTS

Showcasing research by Geetha Bolla and Ashwini Nangia from School of Chemistry, University of Hyderabad, Prof. C.R. Rao Road, Gachibowli, Central University P.O, Hyderabad 500 046, India, CSIR-National Chemical Laboratory, Dr. Homi Bhabha Road, Pune 411 008, India, and Department of Chemical Engineering Massachusetts Institute of Technology, 77 Massachusetts Ave, Cambridge, MA 02139, USA.

Novel pharmaceutical salts of albendazole

Novel molecular salts of the albendazole drug with BSA, PTSA, OA, 2,6-DHBA MLE, LTA, and 2,4,6-THBA are reported. BSA and PTSA salt hydrates are 2D isostructural confirmed by Xpac analysis. Proton transfer to give a salt was confirmed by 15N ss-NMR by tracking the chemical shift of the imidazole N2. These results add to the growing literature on salts and cocrystals of anthelminthic bendazole drugs and will have promising applications in the pharmaceutical industry.

As featured in:
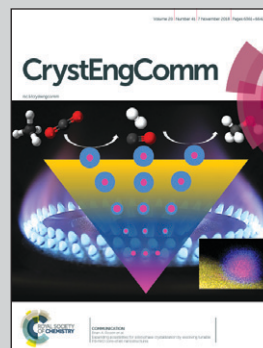
See Geetha Bolla and Ashwini Nangia, *CrystEngComm*, 2018, **20**, 6394.

ROYAL SOCIETY OF CHEMISTRY

rsc.li/crystengcomm

Check for updates

Novel pharmaceutical salts of albendazole†

Geetha Bolla [iD] *[ab] and Ashwini Nangia [iD] *[ac]

Albendazole (ABZ) is a class II safe and effective antihelmintic drug in the benzimidazole group according to the BCS (Biopharmaceutics Classification System) with low solubility (9 mg L^{-1}) and high permeability (log P 2.54). Novel salts and salt hydrates of ABZ are reported with benzene and p-toluene sulfonic acid (BSA, PTSA), as well as carboxylic acids such as oxalic acid (OA), maleic acid (MLE), L-tartaric acid (LTA), 2,6-dihydroxybenzoic acid (2,6-DHBA), and 2,4,6-trihydroxybenzoic acid (2,4,6-THBA). The products ABZ–BSA, ABZ–BSA–H, ABZ–PTSA, ABZ–PTSA–H, ABZ–OA–H and ABZ–2,6-DHBA were confirmed by single crystal X-ray diffraction. In the hydrate structures (designated as –H), the water molecule acts as a bridge in the hydrogen bonding network. The salt formation of ABZ–MLE, ABZ–LTA, and ABZ–2,4,6-THBA was confirmed by ^{15}N ss-NMR based on the chemical shift change of ca. 50 ppm. The sulfonate salt hydrates exhibit 2D isostructurality, and position disorder in the thiopropyl group in the drug crystal structure was not observed in the salts. Crystal lattice energies were calculated for the MLE, LTA, and 2,4,6-THBA complexes of ABZ to confirm the molecular salt formation. The cocrystals of ABZ with the hydroxybenzene carboxylic acids are novel salts in the benzimidazole drugs class.

1. Introduction

Albendazole (ABZ, methyl 5-[propylthio]benzimidazole-2-carbamate) belongs to the benzimidazole family of drugs first marketed by Amedra Pharmaceuticals under the brand name ALBENZA.[1] ABZ is a safe and effective antihelmintic drug (400 mg dose) but has significant antitumor activity in hepatocellular cancer.[2] Benzimidazoles exhibit low erratic availability as a result of its poor aqueous solubility.[3] According to the Biopharmaceutics Classification System (BCS),[4] ABZ is a class II drug of low solubility (9 mg L^{-1}) and high permeability (log P 2.54), representing a dose number of 160 (which means that a single tablet of albendazole will fully dissolve when taken with 160 glasses of 250 mL water).[5] Solid dispersions have been reported to improve the solubility of ABZ, such as polyvinyl pyrrolidone[6] and 2-hydroxypropyl-β-cyclodextrin (HP-β-CD) complexes.[7,8] There are no cocrystals or salts of ABZ reported in the published literature even though it is an essential drug. Two polymorphs, form I and II, of albendazole are reported as tautomers (CSD Refcode SUTWIO, BOGFUZ). There is positional disorder in the thiopropyl chain and tautomerism in

these crystal structures. However, a crystal structure without disorder in the S-C$_3$H$_7$ chain is not reported.[9,10] The positional disorder of the alkyl chain is solved in the crystal structures of the ABZ salts reported in this paper.

2. Experimental

Crystallization of salts

ABZ–BSA (1 : 1) salt. 100.00 mg (0.377 mmol) of ABZ and 59.56 mg (0.377 mmol) BSA were ground in a mortar with a pestle for 30 min after adding 5 drops of nitromethane. The binary crystalline powder was dissolved in CH$_3$NO$_2$ solvent under hot conditions, filtered to remove the undissolved particles and then allowed to crystallize at room temperature. Plate morphology crystals were harvested under ambient conditions after 7 days. Anhydrous ABZ–BSA (1 : 1) salt was further prepared in bulk by nitromethane solvent fast evaporation using a rotary evaporator. Majority of the slow evaporation crystallization experiments in CH$_3$NO$_2$ resulted in a mixture of salt and salt hydrate, and the crystals are of different morphologies.

ABZ–BSA–H (1 : 1 : 1) salt hydrate. 100.00 mg (0.377 mmol) of ABZ and 59.56 mg (0.377 mmol) of BSA were ground in a mortar with a pestle for 30 min after adding 5 drops of water, and then kept for crystallization in a solvent mixture of MeOH and water (1 : 1 v/v) at room temperature. Plate shaped crystals were harvested under ambient conditions after 7 days.

ABZ–PTSA (1 : 1) salt. 100.00 mg (0.377 mmol) of ABZ and 64.70 mg (0.377 mmol) of PTSA were ground in a mortar with a pestle for 30 min after adding 5 drops of MeOH, and then

[a] School of Chemistry, University of Hyderabad, Prof. C.R. Rao Road, Gachibowli, Central University P. O, Hyderabad 500 046, India.
E-mail: bolla.geetha25@gmail.com, ashwini.nangia@gmail.com, ak.nangia@ncl.res.in
[b] Department of Chemical Engineering Massachusetts Institute of Technology, 77 Massachusetts Ave, Cambridge, MA 02139, USA
[c] CSIR-National Chemical Laboratory, Dr. Homi Bhabha Road, Pune 411 008, India
† Electronic supplementary information (ESI) available. CCDC 1834924–1834929. For ESI and crystallographic data in CIF or other electronic format see DOI: 10.1039/c8ce01311j

Table 1 Crystallographic parameters of the ABZ new solid phases in this study

	ABZ–BSA (2:2)	ABZ–BSAH (1:1:1)	ABZ–PTSA (1:1)	ABZ–PTSAH (1:1:1)	ABZ–OAH (1:1:1)	ABZ–2,6-DHBA (2:2)
CCDC no.	1834929	1834924	1834925	1834926	1834927	1834928
Empirical formula	$C_{12}H_{16}N_3O_2S$, $C_6H_5O_3S$	$C_{12}H_{16}N_3O_2S$, $C_6H_5O_3S$, H_2O	$C_{12}H_{16}N_3O_2S$, $C_7H_7O_3S$	$C_{12}H_{16}N_3O_2S$, $C_7H_7O_3S$, H_2O	$C_{12}H_{12}N_3O_2S$, C_2HO_4, H_2O	$C_{12}H_8N_3O_2S$, $C_7H_6O_4$
Formula weight	423.50	441.50	437.52	455.54	369.35	818.74
Crystal system	Triclinic	Triclinic	Monoclinic	Triclinic	Monoclinic	Monoclinic
Space group	$P\bar{1}$	$P\bar{1}$	$P2_1/n$	$P\bar{1}$	$P2_1/n$	$P2_1/n$
T (K)	298	298	298	100	100	100
a (Å)	8.5042(7)	8.9020(6)	15.2992(17)	8.900(5)	5.2659(7)	17.176(5)
b (Å)	9.4678(7)	9.2715(8)	9.7420(9)	9.573(5)	28.337(4)	9.293(3)
c (Å)	26.084(2)	14.2635(12)	15.8825(14)	14.453(8)	11.202(15)	25.789(8)
α (°)	96	84	90.00	83	90	90.00
β (°)	93	89	115	72	93	105
γ (°)	102	63	90.00	63	90	90.00
V (Å^3)	2031.1(3)	1053.47(15)	2135.3(4)	1047.3(10)	1667.8(4)	3958(2)
D_{calcd} (g cm^{-3})	1.385	1.392	1.361	1.445	1.471	1.374
μ (mm^{-1})	0.296	0.292	0.284	0.296	0.237	0.204
θ range	2.66 to 24.71	2.73 to 24.71	2.83 to 26.31	2.68 to 28.31	2.32 to 26.05	1.28 to 24.71
Z/Z'	2	1	1	1	1	2
Range h	−9 to +9	−10 to +10	−16 to +17	−11 to +11	−6 to 6	−20 to +20
Range k	−11 to +11	−10 to +9	−11 to +6	−11 to +10	−33 to 33	−10 to +10
Range l	−30 to +30	−16 to +15	−18 to +15	−18 to +18	−13 to +13	−30 to +30
Reflections collected	13 242	6424	8071	10 722	15 227	35 767
Total reflections	3638	4246	6906	3587	2841	6738
R_1 [$I > 2\sigma(I)$]	0.0740	0.0694	0.0844	0.0639	0.0640	0.0778
wR_2 (all)	0.2090	0.1945	0.2722	0.1748	0.1599	0.2216
Goodness of fit	1.090	1.046	0.991	1.017	1.326	1.100
Diffractometer	Oxford CCD	Smart Bruker Apex-I	Oxford CCD	Smart Bruker Apex-I	Smart Bruker Apex-I	Smart Bruker Apex-I

kept for crystallization in a solvent mixture of 5 mL of MeOH and nitromethane (1:1 v/v) at room temperature. Plate shaped crystals were harvested under ambient conditions after 3–4 days. The anhydrous material ABZ–PTSA (1:1) salt was further prepared in bulk by nitromethane solvent fast evaporation in a rotary evaporator.

ABZ–PTSAH (1:1:1) salt. 100.00 mg (0.377 mmol) of ABZ and 64.70 mg (0.377 mmol) of PTSA were ground in a mortar with a pestle for 30 min after adding 5 drops of water, and then kept for crystallization in a solvent mixture of 5 mL of MeOH and water (1:1 v/v) at room temperature. Plate shaped crystals were harvested under ambient conditions after 7 days.

ABZ–2,6-DHBA (1:1) salt. ABZ, 100.00 mg (0.377 mmol), and 2,6-DHBA, 57.90 mg (0.377 mmol), were ground in a mortar with a pestle with a few drops of MeOH added for 30 min and crystallized in MeOH and nitromethane solvents. IR and PXRD results of the new solid material were different from those of the initial components.

ABZ–2,4,6-THBA (1:1) salt. ABZ, 100.00 mg (0.377 mmol), and 2,4,6 THBA, 62.94 mg (0.377 mmol), were ground in a mortar with a pestle with a few drops of MeOH added for 30 min. Attempts to grow single crystals afforded a precipitate. The IR and PXRD results of the new solid material were different from those of the starting components.

ABZ–MLE (1:1) salt. ABZ, 100.00 mg (0.377 mmol), and MLE, 43.77 mg (0.377 mmol), were ground in a mortar with a –pestle with a few drops of MeOH added for 30 min. The IR

and PXRD results of the new solid material were different from those of the initial components. Attempts to grow single crystals were not successful.

ABZ–LTA (1:1) salt. ABZ, 100.00 mg (0.377 mmol), and D-LTA, 56.55 mg (0.377 mmol), were ground in a mortar with a pestle with a few drops of MeOH added for 30 min. The IR and PXRD results of the new solid material were different from those of the initial components. Attempts to grow single crystals resulted in a precipitate.

Single crystal X-ray diffraction

Single crystal X-ray diffraction was carried out at 298 or 100 K on a Bruker SMART APEX-1 CCD area detector system equipped with a graphite monochromator and a Mo-K$_\alpha$ fine focus sealed tube (λ = 0.71073 Å) operated at 1500 W power (40 kV, 30 mA). A total of 2400 frames were collected at a scan width of 0.3° in the ω mode and an exposure time of 12 s per frame. The frames were integrated with the Bruker SAINT-Plus software using a narrow-frame integration algorithm, and the data was corrected for absorption effects using the multi-scan method (SADABS); further structures were solved and refined using the Bruker SHELX-TL (ref. 11) software. A check of the final crystallographic information file (.cif) was performed using PLATON.[12] A few of the single crystals were mounted on an Oxford Diffraction Gemini X-ray diffractometer (Mo-Kα source, λ = 0.71013 Å) at 298 K. Data
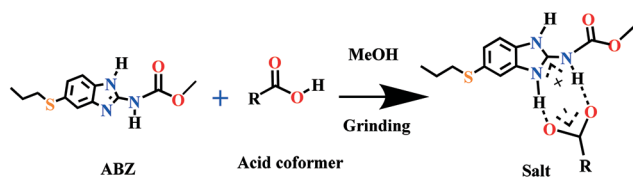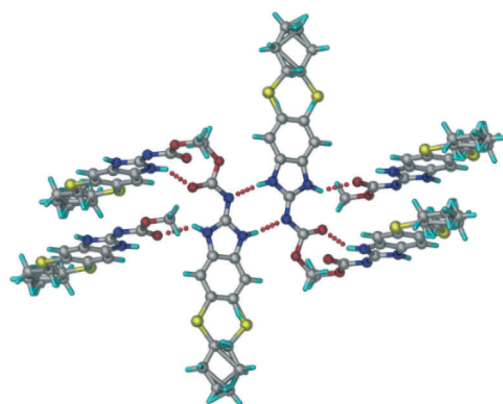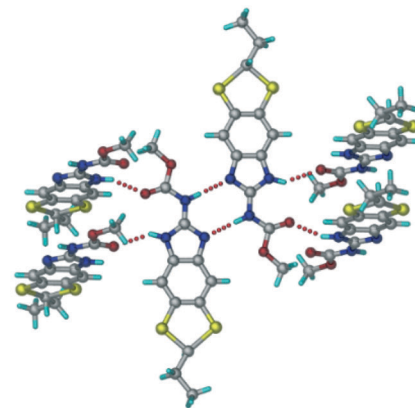
(a)

(b)
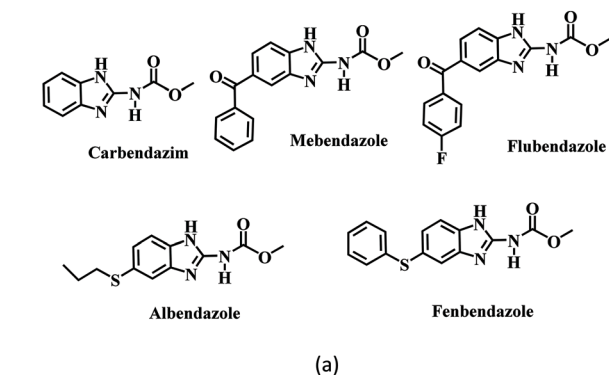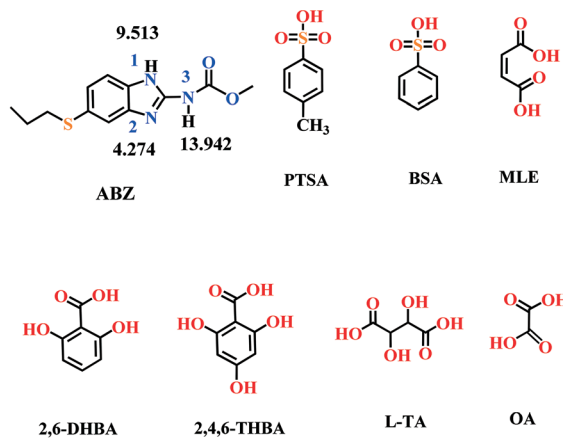
Scheme 1 (a) A few benzimidazole drugs. (b) Chemical structures of ABZ (along with their N pK_a values, will be discussed in later sections) and the coformers reported in this study. (c) Ionic synthon of ABZ with carboxylic acid in an $R_2^2(8)$ motif.

(a)

(b)

Fig. 1 ABZ crystal structures reported in the literature. ABZ exhibits sulphur attached alkyl disorder and the imidazole rings show tautomerism labelled as (a) form II (ref. 9) and (b) form I.[10] CSD ref codes SUTWIO, BOGFUZ.

reduction was performed using CrysAlisPro 171.33.55 software. The X-Seed program[13] and Mercury 3.1 (ref. 14) was used to prepare the final figures and packing diagrams. The crystallographic parameters of both crystal structures are summarized in Table 1. The hydrogen atoms on the heteroatoms (O–H, N–H) were located in the Fourier difference electron density maps for each crystal structure. The hydrogen bond distances (Table S1†) were neutron-normalized to fix the D–H distance to its accurate neutron value in the X-ray crystal structure. Cif files were deposited at the Cambridge Crystallographic Data Centre, CCDC No. 1834924–1834929.

Powder X-ray diffraction

Bulk samples were analyzed by powder X-ray diffraction using a Bruker AXS D8 diffractometer (Bruker-AXS, Karlsruhe, Germany). Experimental conditions: Cu-Kα radiation (λ = 1.5418 Å), 40 kV, 30 mA, scanning interval 5–50° 2θ at a scan rate of 1° min^{-1}, time per step 0.5 s.

Solid-state NMR spectroscopy

Solid-state ^{15}N NMR spectra were recorded on a Bruker Ultra shield 400 spectrometer (Bruker BioSpin, Karlsruhe, Germany). A cross-polarization, magic angle spinning (CP-MAS) pulse sequence was used for spectral acquisition. Each sample was spun at a frequency of 5.0 ± 0.01 kHz, and the magic angle setting was calibrated by the KBr method. Approximately 100 mg of the fine crystalline sample was tightly packed into a zirconia rotor with the help of a Teflon stick up to the Kel-F cap mark. Each data set was subjected to a 5.0 Hz line broadening factor and subsequently Fourier
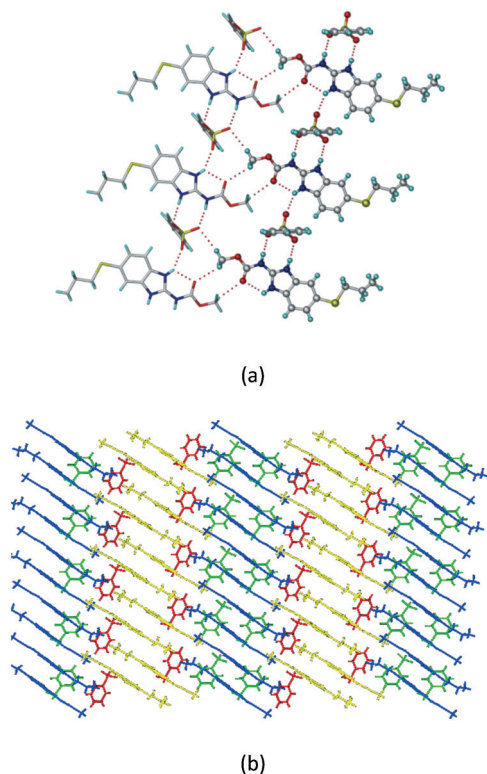
(a)

(b)

Fig. 2 (a) Ionic synthon of sulfonate–imidazole and ester dimers along the *b*-axis. (b) Molecular packing in the ABZ–BSA structure. Symmetry-independent molecules are shown by different shades.

transformed and phase corrected to produce a frequency domain spectrum. ^{15}N CP-MAS spectra were recorded at 40
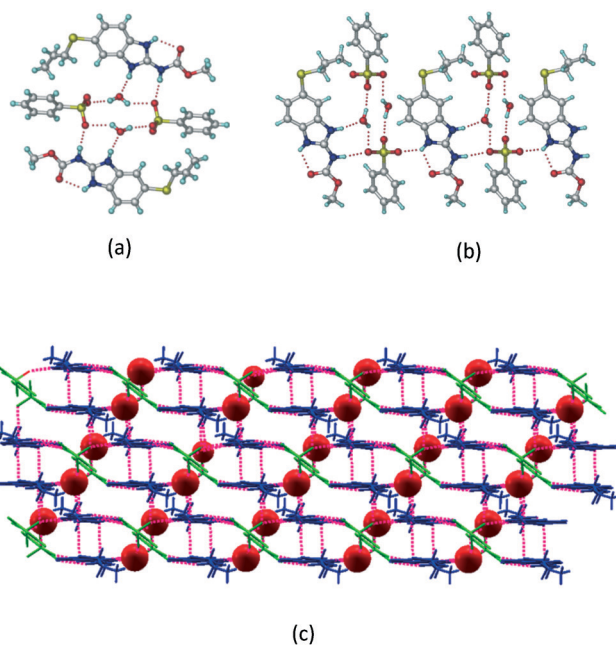

(a)

(b)

(c)

Fig. 3 (a) The bridging water molecules act as proton donors for the sulfonate and acceptors for N$^+$–H resulting in the ring network $R_3^2(8)$ $R_4^4(12)R_3^2(8)$. (b) The sulfonate–water molecules are bonded *via* N–H···O$^-$ hydrogen bonds to ABZ. (c) Complete packing of cations, anions and water molecules.

(a)

(b)

(c)
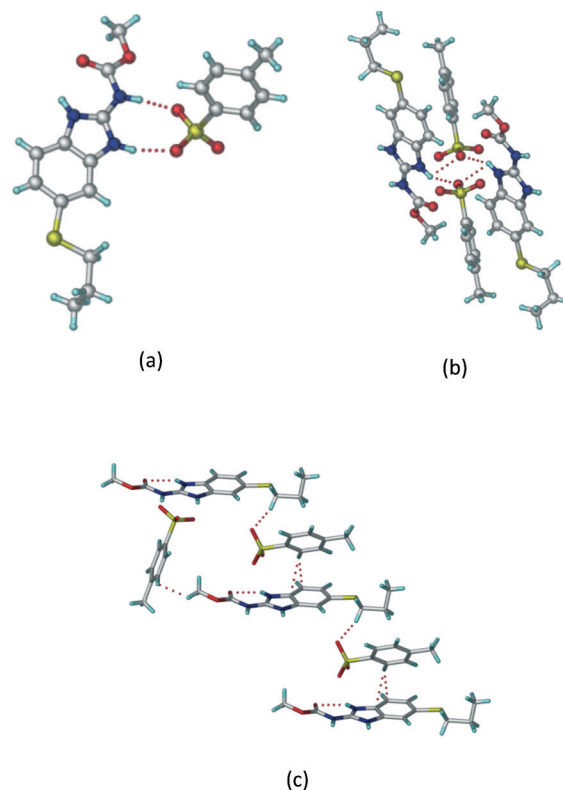
Fig. 4 (a) Proton transfer from *p*-toluenesulfonic acid to the ABZ secondary imidazole N atom results in an $R_2^2(8)$ ring motif in the ABZ–PTSA (1:1) salt. (b) The view of the $R_2^2(8)$ ring motif present in ABZ–PTSA. (c) Bimolecular units of ABZ–PTSA extended through N$^+$–H···O$^-$ interactions along the *b*-axis.

MHz and referenced to glycine N, and then the chemical shifts were recalculated to nitromethane ($\delta_{glycine}$ = −347.6 ppm).

Thermal analysis

DSC experiments were performed using a Mettler Toledo DSC 822e module. Samples were placed in vented aluminum sample pans for DSC. A typical sample size is 4–6 mg for DSC. The temperature range was 30–300 °C at 5 K min^{-1} for DSC. The samples were purged with a stream of dry N$_2$ flowing at 80 mL min^{-1}.

Vibrational spectroscopy

A Thermo-Nicolet 6700 FT-IR spectrometer (Waltham, MA, USA) was used to record the IR spectra. The IR spectra were recorded for the samples dispersed in KBr pellets.

3. Results and discussion

New solid phases of ABZ with different sulfonic acids such as benzenesulfonic acid (BSA) and *p*-toluenesulfonic acid (PTSA) and carboxylic acids such as oxalic acid (OA), 2,6-dihydroxybenzoic acid (2,6-DHBA), 2,4,6-trihydroxybenzoic acid (2,4,6-THBA), maleic acid (MLE) and L-tartaric acid (LTA)
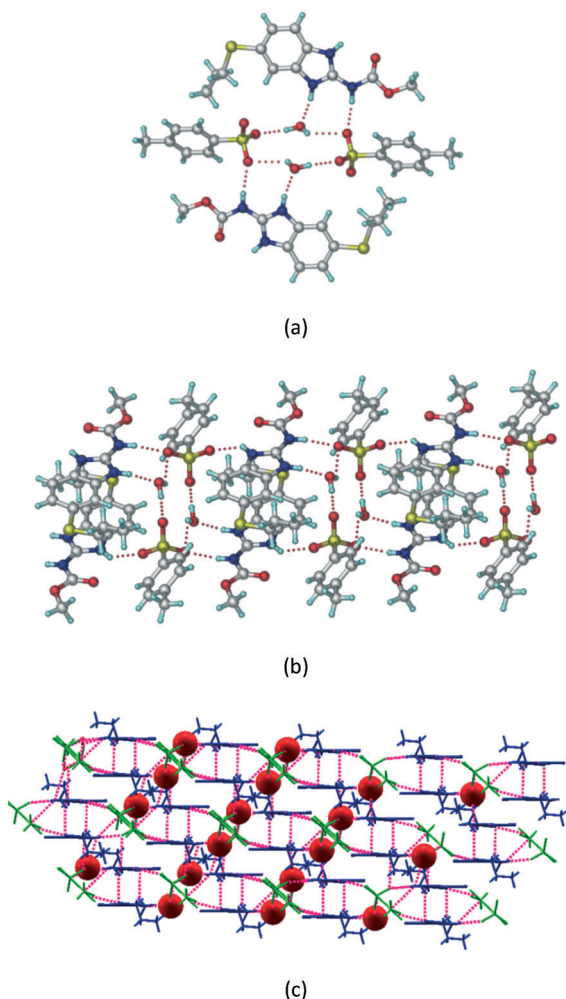
(a)

(b)

(c)

Fig. 5 (a) Bridging water molecules between ABZ and PTSA result in a basic ring unit. (b) The basic motifs are extended *via* N$^+$–H⋯O$^-$ hydrogen bonds along the *a*-axis. (c) 2D packing of the ABZ–PTSAH basic ring motifs resulted in a stacked wave nature as that of ABZ–BSAH.

(a)

(b)

Fig. 6 (a) The carboxylate ion of OA forms a heterodimer with a protonated ABZ 1,3 di N–H moiety resulting in R$_2^2$(8) motifs. (b) 2D packing of ABZ–OA–H results in a successive ladder type of packing.

hydrate exclusively and DHBA an anhydrate salt. Salts of mebendazole with carboxylic acids and sulfonic acids have been reported.[18–20] Similarly, a flubendazole salt with maleic acid was published recently.[21] Even though there are related drugs listed

(a)

(b)

Fig. 7 (a) The basic unit present in the ABZ–2,6-DHBA salt in a 1 : 1 ratio with two molecules in the asymmetric unit. (b) 2D packing of the salt shows adjacent helical nature packing (H atoms are removed for clarity).

were prepared and characterized by IR, PXRD and DSC. The products with BSA, PTSA, OA, and 2,6-DHBA were determined to be salts, confirmed by single crystal X-ray diffraction. Good diffraction quality crystals could not be harvested for ABZ–2,4,6-THBA, ABZ–MLE, and ABZ–LTA, therefore, these phases were confirmed as salts by the chemical shift in their solid-state ^{15}N NMR spectra. A few benzimidazole drugs are shown in Scheme 1a, and the structures of the coformers used in this study are shown in Scheme 1b. The supramolecular synthon in albendazole salts with proton transfer from the carboxylic acid group to the basic benzimidazole nitrogen of the R$_2^2$(8) motif[15–17] is shown in Scheme 1c. The sulfonate salts crystalize as anhydrates and hydrates (designated as –H in name abbreviations) during the solution crystallization experiments (Experimental section). Attempts to prepare an anhydrate salt of BSA was successful the first time, subsequent experiments gave the hydrate. For the carboxylic acid coformers, OA gave a salt
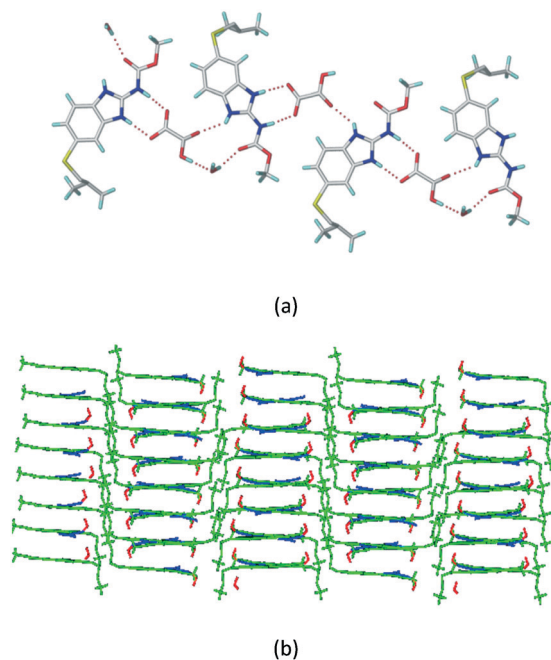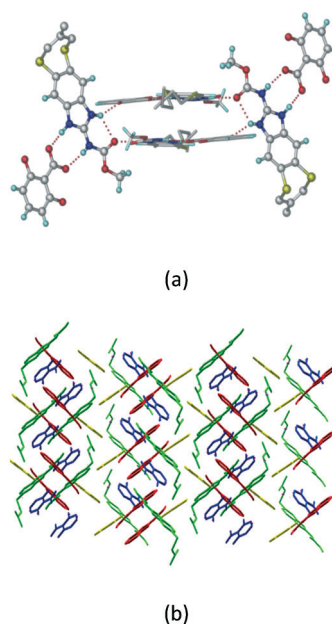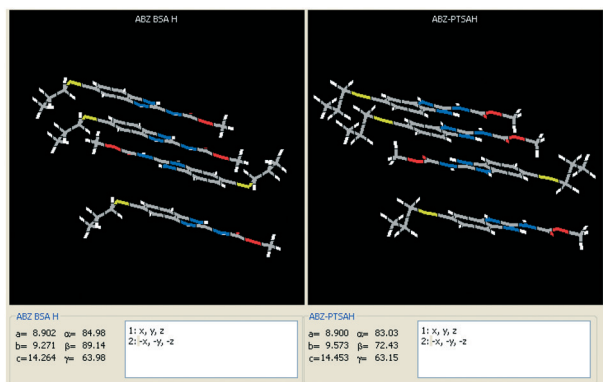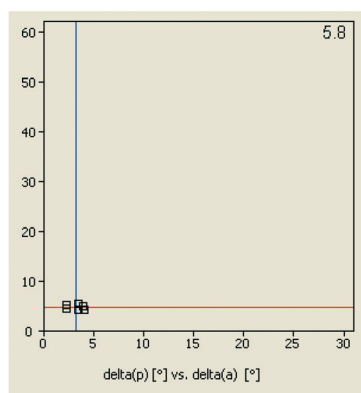
(a)

(b)

Fig. 8 (a) The XPac analysis of ABZ–BSA–H and ABZ–PTSA–H shows that four molecules are identically arranged in the supramolecular construct. (b) The interplanar angular deviation (δp, x-axis) vs. angular deviation (δa, y-axis) plot (in °) indicates a dissimilarity index of 5.8, which confirmed the 2D isostructurality of the two salt hydrates.

in Scheme 1a from literature reports, the crystal structures of albendazole salts are new observations in present study.

Crystal structure analysis

The crystal structures of the two reported polymorphs of albendazole are discussed first.[9] The ABZ molecules form a N–H···N dimer synthon in an $R_2^2(6)$ motif and extend via N–H···O hydrogen bonding to the ester C=O in both crystal

Table 3 Melting points of the ABZ salts from the DSC thermograms

Crystalline form	m.p. (°C) of ABZ/coformer	m.p. (°C) of salt
ABZ	198–202	—
ABZ–BSA (1:1)	103–106	159–170
ABZ–BSA–H (1:1:1)	103–106	83–92, 167–173
ABZ–PTSA (1:1)	103–106	159–170
ABZ–PTSA–H (1:1:1)	103–106	83–92, 167–173
ABZ–OA–H (1:1:1)		57–60, 141–146
ABZ–2,6-DHBA (1:1)	200–205	178–182
ABZ–2,4,6-THBA (1:1)	210–213	144–148
ABZ–MLE (1:1)	135–137	145–147
ABZ–LTA (1:1)	206–209	170–173

structures. The pseudo-symmetry in the molecule due to the imidazole ring results in the disorder of the S–propyl side chain, and the two structures differ in the nature of their side chain disorder (Fig. 1). The two polymorphs are a result of benzimidazole tautomerism, reported for omeprazole polymorphs about a decade ago.[22,23] The hydrogen bonds are stronger in the salts and cocrystals of ABZ (Table S1 for the crystallographic data and Table S2 for the hydrogen bonding details, see the ESI†).

ABZ sulfonate salts

ABZ–BSA (1:1) salt. A salt of ABZ and benzenesulfonic acid (triclinic $P\bar{1}$ space group) was crystallized with the proton transfer between BSA and the imidazole nitrogen resulting in an $R_2^2(8)$ ring motif.[15–17] During the routine solution crystallization experiments in nitromethane, EtOAc, and CH_3CN solvents, the anhydrate and hydrate salts were observed concomitantly. The polymorphs were distinguished by their crystal morphology as plates and rods, which were hand-picked for crystal data collection. The asymmetric unit contains two molecules of ABZ and BSA, and such salt aggregates are connected via C–H···O (C21–H21A···O1 3.139 Å; C9–H9B···O3, 3.164 Å) interactions of the ester dimer $R_2^2(10)$ ring (Fig. 2a). The complete molecular packing is shown in Fig. 2b.

ABZ–BSA–H (1:1:1) salt hydrate. The ABZ–BSA salt crystallization in alcoholic solvents afforded a hydrate, whereas the crystallization in a CH_3NO_2–EtOAc (1:1) solvent mixture resulted in crystals of both the salt and its hydrate. ABZ–BSA–H (1:1:1) crystallized in the triclinic space group $P\bar{1}$. Water

Table 2 FT-IR stretching frequencies (ν_s, cm^{-1}) of the ABZ salts

Crystalline forms	C=O (ester carbonyl of ABZ) cm^{-1}	N–H (Br) cm^{-1}	O–H (Br) for coformer cm^{-1}	Carboxylate/sulfonate (asym) cm^{-1}
ABZ	1712.3	3328.0	—	—
ABZ–BSA–H (1:1:1)	1751.2	3259.7	3374.7	1250.5, 1127.5
ABZ–PTSA (1:1)	1762.1	3453.9	3397.8	1245.7, 1200.7
ABZ–PTSA–H (1:1:1)	1754.5	3458.1	3397.8	1232.5, 1181.8
ABZ–OA–H (1:1:1)	1751.3	3432.7	3439.8	1248.0
ABZ–2,6-DHBA (1:1)	1745.5	3467.2	3475.5	1253.3
ABZ–2,4,6-THBA (1:1)	1730.8	3545.1	3406.8	1144.0
ABZ–MLE (1:1)	1746.0	—	—	1261.3
ABZ–LTA (1:1)	1751.2	3319.3, 3264.5	3402.0	1244.0
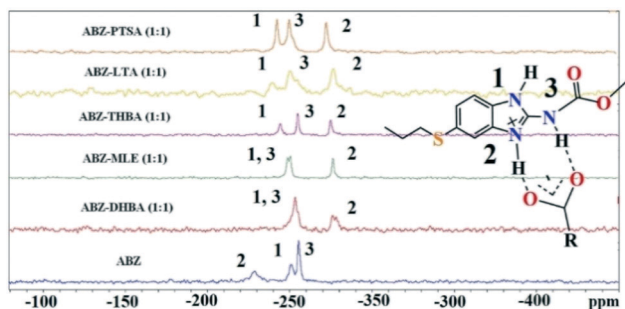
Fig. 9 ^{15}N ss-NMR of the ABZ salts.

Table 5 pK_a values of ABZ and the coformers^a

Name	pK_a	Difference	Result
ABZ	N2 = 4.27, 9.51, −1.80		
BSA	−2.36	6.63	Salt
PTSA	−2.13	6.4	Salt
OA	1.36, 4.11	2.91, 0.16	Salt
2,6-DHBA	1.51	2.76	Salt
2,4,6-THBA	1.82	2.41	Salt
MLE	3.04, 5.91	1.13, −1.64	Salt
LTA	3.86, 5.95	0.14, −1.68	Salt

^{a} pK_a values were calculated considering a water medium using the Marvin pK_a calculator, N2 is the active N for salt formation. https://www.chemaxon.com/marvin/sketch/index.php.

molecules act as a bridge between the ABZ and BSA molecules via N–H···O$^-$ (N3–H3A···O3, 2.798(4) Å, 173°), N–H···O (N1–H1A···O6, 2.687(4) Å, 169°) and O–H···O$^-$ (O6–H6A···O4, 2.686(6) Å, 162°; O6–H6B···O3, 2.834(4) Å 134°) bonds affording a network of R$_3^2$(8)R$_4^4$(12)R$_3^2$(8) ring motifs (Fig. 3a). BSA and water ring motifs are sandwiched between the ABZ molecules and connected via N$^+$–H···O$^-$ hydrogen bonds (Fig. 3b). The schematic packing with water shown as red spheres is shown in Fig. 3c.

ABZ–PTSA (1:1) salt. Crystals of the ABZ–PTSA (1:1) salt were obtained in nitromethane/EtOAc solvent (1:1 v/v) in the space group $P2_1/n$. The proton transfer from PTSA to the imidazole nitrogen atom of ABZ results in an R$_2^2$(8) ring motif via imidazole N–H···O$^-$ (N1–H1A···O4, 2.763(5) Å, 169°) and amide N–H···O$^-$ (N3–H3A···O3, 2.703(5) Å, 164°) bonding with the sulfonate oxygen atoms of PTSA (Fig. 4a). The dimers of these units extend along the b-axis as chains. The imidazolium N$^+$–H donor and O$^-$ acceptor of PTSA form an R$_2^2$(8) motif with bifurcated (N2–H2A···O5, 2.820(5) Å, 146°) hydrogen bonds (Fig. 4b). Additionally, these binary adducts make 1D chains which extend through C–H···O$^-$ (C10–H10B···O3, 3.309(9) Å, 142°) and C–H···π (C9–H9A···π of PTSA, 2.932 Å; C18–H18···π of ABZ, 3.262 Å) interactions (Fig. 4c).

ABZ–PTSA–H (1:1:1) salt hydrate. In addition to ABZ–PTSA, the salt hydrate ABZ–PTSA–H (1:1:1) crystallized (P$\bar{1}$ space group) after a few crystallization cycles. The proton is transferred from PTSA to the imidazole nitrogen of ABZ (Fig. 5a). The hydrogen bonding in this structure is similar to that of the ABZ–BSA–H salt and also showed 2D iso-structurality (Fig. 8). The calculated dissimilarity index of 5.8 confirms the 2D iso-structurality^{24,25} between them. The water molecule acts as a bridge between the ABZ and PTSA molecules via N–H···O$^-$ (N3–H3A···O4, 2.865(4) Å, 175°); N–H···O

(N1–H1A···O6, 2.665(4) Å, 174°) and O–H···O$^-$ (O6–H6A···O3, 2.678(4) Å, 141°; O6–H6B···O4, 2.747(3) Å 145°) hydrogen bonds in the R$_3^2$(8)R$_4^4$(12)R$_3^2$(8) motif. The oxygen of PTSA is connected through N$^+$–H···O$^-$ (N2–H2A···O5 2.790(4) Å, 142°) H-bonds (Fig. 5b). Such motifs extend along the b-axis in a double helical structure and helical sheets (Fig. 5c).

ABZ carboxylate salts

ABZ–OA–H (1:1:1) salt hydrate. The dimers of ABZ are interrupted by oxalic acid coformers (P2_1/n space group). One of the OA protons is transferred to ABZ resulting in ABZ–OA–H, and the second COOH of OA is neutral. Heterodimers of the ABZ and OA are assembled via N–H···O$^-$ and N–H···O (N1–H1A···O4, 2.671(4) Å, 171°; N3–H3A···O3, 2.689(4) Å, 174°) hydrogen bonds in the R$_2^2$(8) motif (Fig. 6a). The neutral COOH of the OA bonds with the second N–H of ABZ and water molecules through N$^+$–H···O$^-$ and O–H···O$^-$ (N2–H2A···O5, 2.786(4) Å, 139°; O7–H7B···O1, 2.859(4) Å, 154°) hydrogen bonds (Fig. 6b).
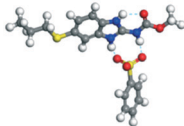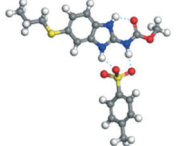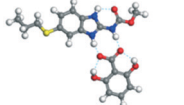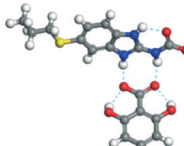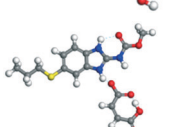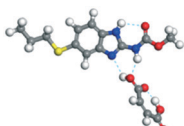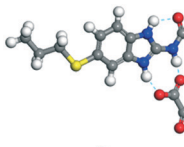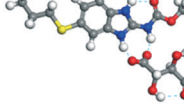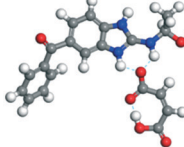
ABZ–2,6-DHBA (1:1) salt. Cations of ABZ assemble with the carboxylate of 2,6-DHBA by N–H···O$^-$ (N3–H3A···O$^-$4, 2.649(5) Å, 173°; N1–H1A···O$^-$6, 2.703(4) Å, 175°; N5–H5A···O$^-$11, 2.696(5) Å, 179°; N6–H6A···O12 2.680(5) Å, 169°) hydrogen bonds forming an R$_2^2$(8) motif involving two molecules each in the asymmetric unit (space group $P2_1$/n) (Fig. 7a, shaded differently). The molecular planes are inclined at 77.9°, and such units extend via N$^+$–H···O hydrogen bonds. 1D chains extend via weak C–H···π interactions to construct 2D sheet structures. The sulfur atom and n-butyl chains in the two molecules are split and modelled using the PART command. The hydrogen atoms attached to the alkyl chain are disordered.

IR spectroscopy

The infrared spectroscopy^{26,27} results of ABZ showed characteristic peaks of an ester carbonyl (1712.3 cm^{-1}) and a N–H stretch (3328.0 cm^{-1}). The new solid phases ABZ–MA, ABZ–LTA, ABZ–2,6 DHBA, ABZ–2,4,6 THBA, ABZ–BSA, ABZ–PTSA and ABZ–PTSA–H exhibited a shift in their IR bands when compared to the starting materials. The red shift in the C=O and N–H frequency peaks indicates stronger hydrogen

Table 4 ^{15}N ss-NMR chemical shifts (ref. $\delta_{glycine}$−347.6 ppm) of the ABZ salts. The protonated N2 site column is formatted in bold

Salt	δ N1	δ N2	δ N3
ABZ	−255.49	**−228.96**	−250.88
ABZ–2,6-DHBA (1:1)	−249.26	**−274.14**	−272.02
ABZ–2,4,6-THBA (1:1)	−244.37	**−274.97**	−254.94
ABZ–MLE (1:1)	−248.88	**−276.38**	−250.42
ABZ–LTA (1:1)	−242.01	**−277.99**	−250.06
ABZ–PTSA (1:1)	−245.79	**−275.75**	−253.23

Table 6 Energy stabilization calculations for ABZ, the coformers and salts with their structures

S. No.		Calculated energy kcal mol^{-1}	$\Delta E = E_{complex} - (E_{ABZ} + E_{coformer})$ kcal mol^{-1}	Adduct structure
1	ABZ	−116.57		—
2	BSA	−7.12	−154.81 − (−123.70) = −31.11	
3	PTSA	−14.93	−165.50 − (−131.50) = −34.00	
4	2,6-DHBA	−55.56	−224.41 − (−172.14) = −52.27	
5	2,4,6-THBA	−78.58	−247.45 − (−195.16) = −52.29	
6	MLE	−62.05	Salt −285.35 − (−178.63) = −106.72	
			Co-crystal −187.32 − (−178.63) = −8.69	
7	OA	24.82	−145.38 − (−91.75) = −53.63	
8	LTA	20.72	−139.93 − (−95.84) = −44.09	
9	MBZ–MLE VEVPUJ ref. 18	MBZ −70.82 MLE −62.05	−227.49 − (−132.87) = −94.62	

bonding (spectra are shown in Fig. S1, ESI† and values are listed in Table 2). Chen et al.[18] reported an MEB–MLE salt peak at 1745 cm^{-1} which is comparable with that of the ABZ–MLE adduct at 1746 cm^{-1}.

Powder X-ray diffraction

Powder X-ray diffraction[28–30] is the most frequently used technique to establish the formation of new crystalline materials. Quick comparison of the fingerprints of the product phase (cocrystal/salt) and the starting material peaks (drug, coformer) is done by visual inspection of the diffraction line patterns. The powder pattern of ABZ, the ground material with coformers, and the coformer plots indicate new sets of peaks. The bulk phase powder patterns of ABZ–BSA–H, ABZ–PTSA, ABZ–PTSA–H, ABZ–OA–H and ABZ–2,6-DHBA matches those of the calculated X-ray lines for the salts from the crystal structures (Fig. S2a–e, ESI†). A PXRD comparison of the ground material diffraction pattern of ABZ–2,4,6-THBA, ABZ–MLE and ABZ–LTA showed unique peaks at 2θ values which confirmed the new crystalline phases (Fig. S2f–h, ESI†).
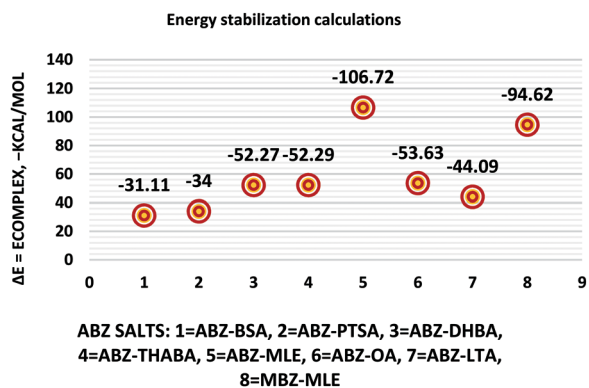
Fig. 10 Energy stabilization plot of the ABZ salts.

Thermal analysis

A different melting point of the cocrystal/salt in the DSC thermogram is indicative of a new phase. The ABZ commercial sample used in the experiments melts at 198–202 °C; the DSC endotherms of the ABZ salts are shown in Fig. S3, ESI.† The melting points of the products along with their coformers are listed in Table 3. ABZ–MLE and ABZ–PTSA showed melting points in between those of their two components, whereas ABZ–LTA, ABZ–2,6-DHBA, and ABZ–2,4,6-THBA melted below their components' melting temperature.

Solid state NMR (ss-NMR)

Solid state NMR of the polymorphs and cocrystals[31–34] provides information about the short range order and hydrogen bonding. The positions of the hydrogen atoms in the crystalline molecular compounds exhibiting partial charge transfer are difficult to locate in the absence of X-ray diffraction. It is more complicated if the crystal structures of the organic solids are not available. The difficulty of growing good quality single crystals leads to the situation that ^{15}N ss-NMR becomes an alternative choice to better understand their structure, even though neutron diffraction can produce more precise data, it is not routinely accessible using a laboratory diffractometer. However, ^{15}N ss-NMR is challenging because the ^{15}N isotope has a low natural abundance (0.368%). The difference in the chemical shifts (Δppm) of ^{15}N is correlated with those of the salts to assess the hydrogen bond strength. Li *et al.* showed that ^{15}N ss-NMR could be used for monitoring a cancer drug in dicarboxylic cocrystals and salts. Those reported results ranged from no transfer to partial transfer to complete transfer of the proton on the aromatic N of ABZ and ss-NMR was used to compare the single crystal structures.[34] In addition, they showed that the N–H and N···O distances are a function of the difference in their ^{15}N ss-NMR chemical shifts, Δppm of −20 to −60 for no proton transfer and −60 to −120 for proton transfer. The neutral N–H of imidazole was assigned as atom 1, protonated N–H as 2 and the carbamate N as atom 3 (Fig. 9, Table 4). ^{15}N ss-NMR of the ABZ–PTSA salt (for which the single crystal data are available to confirm the salt state) and ABZ–LTA,

ABZ–MLE, and ABZ–2,4,6-THBA (single crystal data could not be recorded) allowed the salt structure of ABZ to be assigned based on the chemical shift of the ^{15}N (protonated) peak, which was at −274.14 ppm for ABZ–2,6-DHBA, −274.97 ppm for ABZ–2,4,6-THBA, −276.38 ppm for ABZ–MLE, −277.99 ppm for ABZ–LTA, and −275.75 ppm for ABZ–PTSA (for full chemical shift values see Table 4, −228.96 ppm for ABZ). N2 is involved in the protonation, hence an upfield shift is observed from −228 to ≃275 ppm, whereas the other N atoms N1 and N3 were not involved in the protonation, but the hydrogen packing interactions changed when compared with the starting ABZ which resulted in a small change in ppm in the spectrum.

ΔpKₐ rule

The ΔpK_a rule[35–37] predicts the product as cocrystal or salt based on the pK_a of acid and base reacted during cocrystallization. If ΔpK_a = pK_a (conjugate acid of the base) − pK_a (acid) is less than 0, the result is a cocrystal, a ΔpK_a > 3 will result in a salt, and the range 0 < ΔpK_a < 3 is an intermediate or grey zone of different proton states. The formation of salts in this study is consistent with a ΔpK_a > 3. The pK_a values were calculated using a Marvin pK_a calculator considering a water medium[38] (Table 5). The pK_a range for the intermediate zone is continuously updated as additional data is made available, *e.g.* from the Cambridge Structural Database.[39]

Complexation calculations

The molecular structure geometry was optimized by using the COMPASS II force field in Materials Studio. The association energy was calculated as the difference in energy of the optimized complex and the combined energy of the optimized individual molecules where $E_{complex}$ is the energy of the optimized molecular complex, E_{ABZ} is the energy of the optimized ABZ molecule, and $E_{coformer}$ is the energy of the optimized coformer (eqn (1)). The sulfonate salts reported in present study showed that, they are stabilized by −30 to −35 kcal mol^{-1} whereas carboxylates are stabilized by −50 kcal mol^{-1} (except LTA, −44 kcal mol^{-1}) during complex formation. However, MLE salt has the highest complexation energy of −106 kcal mol^{-1}. This means that complexes of the carboxylate salts are more stable than those of the sulfonates. The stabilization energy of the ABZ–MLE cocrystal (no proton transfer) at −8.69 kcal mol^{-1} is much less compared to those of the mebendazole–maleic acid, and ABZ–MLE salts (−94.62, −106.72 kcal mol^{-1}, with proton transfer). Based on the ss-NMR results and the calculated complexation energies, we surmise that ABZ–MLE is a salt, Table 6, Fig. 10.

$$\Delta E = E_{complex} - (E_{ABZ} + E_{coformer}) \qquad (1)$$

Salts and cocrystals of bendazole drugs reported in the literature

Mebendazole (MBZ) is an anthelmintic drug in the bendazole family. ABZ and MBZ differ in the substitution on the

Table 7 Literature reports of bendazole salts and cocrystals with their name, CSD Refcode, reference and packing
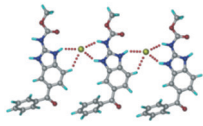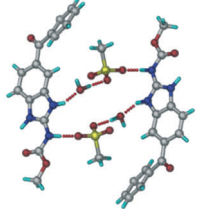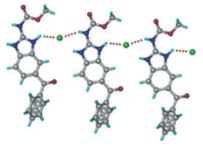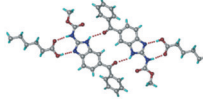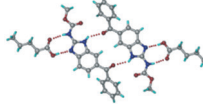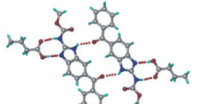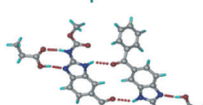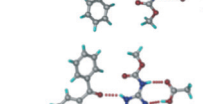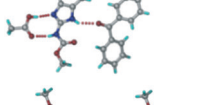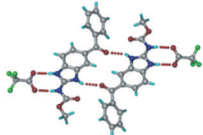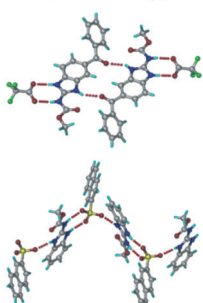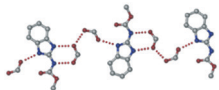
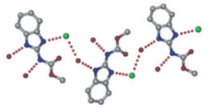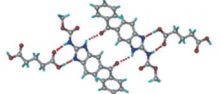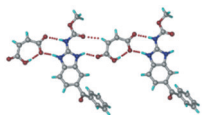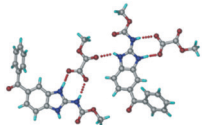| S. No.	Compound name, CSD Refcode	Crystal structure	Adduct	Reference
1	Mebendazole–hydrobromide, BMCBIB		Salt	40
2	Mebendazole mesylate monohydrate, MIJDIU		Salt	41
3	Mebendazole hydrochloride, NIZCIJ		Salt	42
4	Mebendazole hexanoic acid, PIDJOD		Co-crystal	20
5	Mebendazole pentanoic acid, PIDJUJ		Co-crystal	20
6	Mebendazole butanoic acid, PIDKAQ		Co-crystal	20
7	Mebendazole propionic acid, SAGQEW		Co-crystal	20
8	Mebendazole acetic acid, PIDKEU		Co-crystal	20
9	Mebendazole formate formic acid, PIDKIY		Salt co-crystal adduct	20
10	Mebendazole trifluoroacetate, PIDKOE		Salt	20
11	2-(Methoxy carbonylamino) benzimidazolium naphthalene-1-sulfonate, QESBOG		Salt	43

Table 7 (continued)

S. No.	Compound name, CSD Refcode	Crystal structure	Adduct	Reference
12	Methyl N-(1,3-benzimidazolium-2-yl)carbamate formate formic acid, RAVLAC		Salt co-crystal adduct	44
13	Methyl N-(1,3-benzimidazolium-2-yl)carbamate chloride dihydrate, RAVLEG		Salt	44
14	Mebendazole glutaric acid, VEVPOD		Cocrystal	18
15	Mebendazole maleic acid, VEVPUJ		Salt	18
16	Mebendazole methoxy(oxo)acetate, VEVQAQ		Salt	18

benzene portion, and MBZ–MLE salt crystal structures have been reported.[18] MBZ forms a salt-cocrystal continuum adduct with formic acid, MBZH$^+$–FA$^-$–FA, and a salt with trifluoroacetic acid, whereas with other homologous acids such as acetic, propionic, butanoic, pentanoic, and hexanoic acids, it formed cocrystals.[20] Bendazole salts with HCl, HBr, sulfonic acids such as methane, benzene, toluene, and naphthalene, and aliphatic carboxylic acids such as formic, maleic and oxalic have been reported.[40–44] (Table 7) We present new salts of L-tartaric acid and hydroxy benzoic acids with ABZ in addition to those from previous studies.

4. Conclusions

New salts of the albendazole drug with BSA, PTSA, OA, 2,6-DHBA MLE, LTA, and 2,4,6-THBA are reported. The salts of BSA, PTSA, OA, and 2,6-DHBA were confirmed by single crystal diffraction whereas others were characterized through powder X-ray diffraction, IR and ss-NMR and DSC. In addition, BSA, PTSA and OA crystallize as hydrates, and anhydrates during crystallization were observed. The BSA and PTSA salt hydrates are 2D isostructural, confirmed by Xpac analysis. The ABZ butyl chain disorder observed in the parent structure is resolved in the salt crystal structures except in ABZ–2,6-DHBA. Proton transfer to afford a salt was confirmed by ^{15}N ss-NMR by tracking the chemical shift of the imidazole N2 peak in the MLE, LTA and 2,4,6-THBA salts. The salt formation of ABZ–MLE was further confirmed by comparing the complexation energy of ABZ–MLE with that of MBZ–MLE. The ΔpK_a rule of 3 was followed in the present study. These results add to the growing literature on the salts and cocrystals of anthelminthic bendazole drugs.

Conflicts of interest

The authors declare no competing financial interest.

Acknowledgements

References

1. H. Mohammad, E. Pourgholami, A. Javed, W. E. Lisa, L. E. Ying and L. David, *Cancer Chemother. Pharmacol.*, 2005, **55**, 425–432.
2. J. A. Bogan and S. E. Marriner, *Vet. Res. Commun.*, 1983, **7**, 271.
3. K. Anand and S. Wakode, *Int. J. Chem. Stud.*, 2017, **5**, 350–362.
4. https://tsrlinc.com/resources/services/ (dated 24/07/2018).
5. N. Jagadeeshbabu and A. Nanga, *Cryst. Growth Des.*, 2011, **11**, 2662–2679.
6. S. Torrado, J. J. Torrado and R. Cadórniga, *Int. J. Pharm.*, 1996, **140**, 247–250.
7. V. L. Bassani and D. Kriege, *J. Inclusion Phenom. Mol. Recognit. Chem.*, 1996, **25**, 149–152.
8. C. Moriwaki, G. L. Costa, C. N. Ferracini, F. F. Moraes, G. M. Zanin, E. A. G. Pineda and G. Matioli, *Braz. J. Chem. Eng.*, 2008, **25**, 255–267.

9 B. R. Pranzno, D. Cruickshank, M. Coruzzi, M. R. Caira and R. Bettini, *J. Pharm. Sci.*, 2010, **99**, 3731–3742.

10 https://www.ccdc.cam.ac.uk/structures/search?sid=ConQuest&coden=001078&year=2007&pid=ccdc:668711&aulast=Alhalaweh.

11 *SMART, version 5.625 and SHELX-TL, version 6.12*, BrukerAXS Inc., Madison, Wisconsin, 2000.

12 *PLATON, A Multipurpose Crystallographic Tool*, ed. A. L. Spek, Utrecht University, Utrecht, The Netherlands, 2002; A. L. Spek, *J. Appl. Crystallogr.*, 2003, **36**, 7.

13 *X-Seed, Graphical interface to SHELX-97 and POV-Ray, Program for Better Quality of Crystallographic Figures*, ed. L. J. Barbour, University of Missouri-Columbia, Columbia, Missouri, 1999.

14 https://www.ccdc.cam.ac.uk/Community/csd-community/freemercury/.

15 M. C. Etter and J. C. Mcdonald, *Acta Crystallogr., Sect. B: Struct. Sci.*, 1990, **46**, 256.

16 J. Bernstein, R. E. Davis, L. Shimoni and N. L. Chang, *Angew. Chem., Int. Ed. Engl.*, 1995, **34**, 1555.

17 M. C. Etter and J. C. Macdonald, *Acta Crystallogr., Sect. B: Struct. Sci.*, 1990, **46**, 256–262.

18 J. Chen, Z. Wang, C. Wu, S. Li and T. Lu, *CrystEngComm*, 2012, **14**, 6221–6229.

19 K. D. Paula, G. E. Camí, E. V. Brusau, G. E. Narda and J. Ellena, *J. Pharm. Sci.*, 2013, **102**, 3528–3538.

20 J. Chen and T. Lu Chin, *J. Chem.*, 2013, **31**, 635–640.

21 G. L. B. de Araujo, F. F. Ferreira, C. E. S. Bernardes, J. A. P. Sato, O. M. Gil, D. L. A. Faria, R. Loebenberg, S. R. Byrn, D. D. M. Ghisleni, N. A. Bou-Chacra, T. J. A. Pinto, S. G. Antonio, H. G. Ferraz, D. Zemlyanov, D. S. Gonçalves and M. E. M. Piedade, *Cryst. Growth Des.*, 2018, **18**, 2377–2386.

22 P. M. Bhatt and G. R. Desiraju, *Chem. Commun.*, 2007, 2057–2059.

23 M. K. Mishra, U. Ramamurty and G. R. Desiraju, *J. Am. Chem. Soc.*, 2015, **137**, 1794–1797.

24 T. Gelbrich and M. B. A. Hursthouse, *CrystEngComm*, 2005, **7**, 324–336.

25 T. Gelbrich and M. B. Hursthouse, *CrystEngComm*, 2006, **8**, 448–460.

26 R. M. Silverstein, *Spectrometric Identification of Organic Compounds*, John Wiley & Sons, Inc., 6th edn, 2002, pp. 71–143.

27 R. K. Gilpin and W. Zhou, *Vib. Spectrosc.*, 2005, **37**, 53.

28 S. Karki, T. Friščić, L. Fábián and W. Jones, *CrystEngComm*, 2010, **12**, 4038–4041.

29 J. F. Remenar, M. L. Peterson, P. W. Stephens, Z. Zhang, Y. Zimenkov and M. B. Hickey, *Mol. Pharmaceutics*, 2007, **4**, 386–400.

30 V. André, A. Fernandes, P. P. Santos and M. T. Duarte, *Cryst. Growth Des.*, 2011, **11**, 2325–2334.

31 F. G. Vogt, J. S. Clawson, M. Strohmeier, A. J. Edwards, T. N. Pham and S. A. Watson, *Cryst. Growth Des.*, 2009, **9**, 921–937.

32 P. Sanphui, G. Bolla, A. Nangia and V. Chernyshev, *IUCrJ*, 2014, **1**, 136–150.

33 L. Zhao, M. P. Hanrahan, P. Chakravarty, A. G. DiPasquale, L. E. Sirois, K. Nagapudi, J. W. Lubach and A. J. Rossini, *Cryst. Growth Des.*, 2018, **18**, 2588–2601.

34 Z. J. Li, Y. Abramov, J. Bordner, J. Leonard, A. Medek and A. V. Trask, *J. Am. Chem. Soc.*, 2006, **128**, 8199–8210.

35 C. B. Aakeröy, M. E. Fasulo and J. Desper, *Mol. Pharmaceutics*, 2007, **4**, 317–322.

36 B. Sarma, N. K. Nath, B. R. Bhogala and A. Nangia, *Cryst. Growth Des.*, 2009, **9**, 1546–1557.

37 S. L. Childs, G. P. Stahly and A. Park, *Mol. Pharmaceutics*, 2007, **4**, 323–338.

38 https://www.chemaxon.com/marvin/sketch/index.php (dated 05-04-2018).

39 A. J. Cruz-Cabeza, *CrystEngComm*, 2012, **14**, 6362–6365.

40 N. M. Blaton, O. M. Peeters and C. J. De Ranter, *Cryst. Struct. Commun.*, 1980, **9**, 181–186.

41 K. D. Paula, G. E. Cami, E. V. Brusau, G. E. Narda and J. Ellena, *J. Pharm. Sci.*, 2013, **102**, 3528–3538.

42 E. V. Brusau, G. E. Cami, G. E. Narda, S. Cuffini, A. P. Ayala and J. Ellena, *J. Pharm. Sci.*, 2008, **97**, 542.

43 K. Sepassi, G. S. Nichol and S. H. Yalkowsky, *Acta Crystallogr., Sect. E: Struct. Rep. Online*, 2006, **62**, o5172–o5173.

44 K. K. Turgunov, A. G. Tozhiboev and B. Tashkhodzhaev, *J. Struct. Chem.*, 2005, **46**, 342.